Piezo-Phototronic Enhanced UV Sensing Based on a Nanowire Photodetector Array

Xun Han, Weiming Du, Ruomeng Yu, Caofeng Pan, and Zhong Lin Wang**

Optoelectronic processes in various emerging applications, such as wearable electronics, Internet of things, human–machine interface, implantable medical instruments, and smart sensor networks,[1] highly depend on the performances of photodetectors (PDs).[2] To fulfill the rapidly growing demands of high-performance photosensing devices, tremendous efforts have been devoted to achieve large-scale PDs with high photoresponsivity,[3] adequate spatial resolution,[4] and fast response time.[5] Integration of nanowire PDs into array configuration is a promising solution. As a direct band semiconductor with wide gap of 3.37 eV, ZnO nanowires (NWs) become prospective building blocks[6] and have been extensively investigated for ultraviolet (UV) sensing applications.[3a,7] The piezo-phototronic effect, (known as a three-way coupling of piezoelectric polarization, semiconductor properties, and optical excitation)[8] has been introduced in ZnO[9] and other wurtzite-structured piezoelectric semiconductors,[10] and has led to novel fundamental phenomena and unprecedented device characteristics, as well as applications.[11] Piezoelectric polarization charges created upon straining can effectively modify the energy band diagram at local interface/junction and tune/control the optoelectronic processes of charge carriers, such as generation, recombination, separation, and transport.[9,12]

Here, we demonstrate an UV PD array consisting of 32 × 40 pixels based on vertically aligned ZnO NWs. Each pixel is composed of ZnO NWs and Au nanopatterns to form a Schottky-contacted UV PD with spatial resolution of 100 μm (254 dpi), response time of 62 ms under 3.949 mW cm^{-2} UV illuminations. By introducing the piezo-phototronic effect, the strain-induced piezoelectric polarization charges effectively enhance the performances of the UV PD array by 700% in photoresponsivity, 600% in sensitivity, and 280% in detection limit. The physical mechanism is carefully investigated by analyzing the energy band diagrams at the local metal–semiconductor (M–S) interface under mechanical deformations. This work provides a practical solution to achieving large-scale PDs with high performances by integrating NW-PD into array configuration. The photodetectors array may have applications in optoelectronic systems, biomedical diagnostics, adaptive optical computing, and communication.

The structure of the UV PD array is schematically indicated in **Figure 1**a, together with an optical image of the as-fabricated device as in the inset. Each device is consisting of 32 × 40 pixels as an integration of ZnO NWs photodetectors array. The schematic illustration and the corresponding optical images of the fabrication processes are presented in Figure 1b,c. Indium tin oxide (ITO) strips with 30 μm in width and 70 μm in spacing are deposited on precleaned glass substrate as the bottom electrodes. The pixels of the PD array are defined by depositing a layer of Au and ZnO patterns sequentially to form the Schottky contacts. ZnO NWs arrays are synthesized on top of the seed layer through a low-temperature hydrothermal method, and characterized by X-ray diffraction (Figure S1, Supporting Information) and scanning electron microscopy (SEM) (Figure 1d). The spatial resolution of the UV PD array is derived as 100 μm (254 dpi) by designing the ZnO-NWs pattern with 20 μm × 20 μm in dimension and 80 μm in spacing. Better resolution can be achieved by fabricating the device with finer mask to reduce the dimension and the spacing of ZnO-NWs array. Then, a layer of SU-8 photoresist is spin-coated on the as-prepared NW array (Figure 1e,f) followed by oxygen plasma cleaning to remove the residual photoresist and expose the tips of the NWs. Finally, a layer of Au patterns and a layer of ITO strips orthogonal to the bottom electrodes are deposited as the top electrodes. Each overlapping node between top and bottom electrodes corresponds to a pixel of the UV PD array. Detailed fabrication processes are found in the Experimental Section.

The UV response of a single pixel was investigated to demonstrate the photosensing performances of the PD array by applying 365 nm optical stimuli as summarized in **Figure 2**. The typical *I–V* characteristics of one single pixel in the dark and under UV illuminations at various intensities are shown in Figure 2a, by applying a triangular wave across the device swiping from −2 to +2 V. It is obvious that the output currents increased on applying stronger illumination at both −2 and +2 V biased voltages. For example, at +2 V, the current increases from 9.46 (dark) to 11.84 μA (0.019 mW cm^{-2}), and further to 90.08 μA (8.36 mW cm^{-2}). Upon illumination, the photogenerated holes migrate to the surface of ZnO NWs to discharge the negatively charged oxygen ions [$h^+ + O_2^- = O_2$ (g)], with the photogenerated electrons remaining, and thus resulting in an increase in the charge carrier concentration and a decrease in the width of the depletion layer.[13] The accumulated electrons at the local M–S interface reduce the Schottky barrier height (SBH) from Φ_{SB} to Φ_{SB}^{ill} (Figure S2, Supporting Information), and therefore lead to the increased output currents as observed in Figure 2a. The response time of the UV PD array was investigated by periodically applying different UV

X. Han, W. Du, Prof. C. Pan, Prof. Z. L. Wang
Beijing Institute of Nanoenergy and Nanosystems
Chinese Academy of Sciences
Beijing 100083, China
E-mail: cfpan@binn.cas.cn;
zhong.wang@mse.gatech.edu
R. Yu, Prof. Z. L. Wang
School of Materials Science and Engineering
Georgia Institute of Technology
Atlanta, GA 30332-0245, USA

DOI: 10.1002/adma.201502579

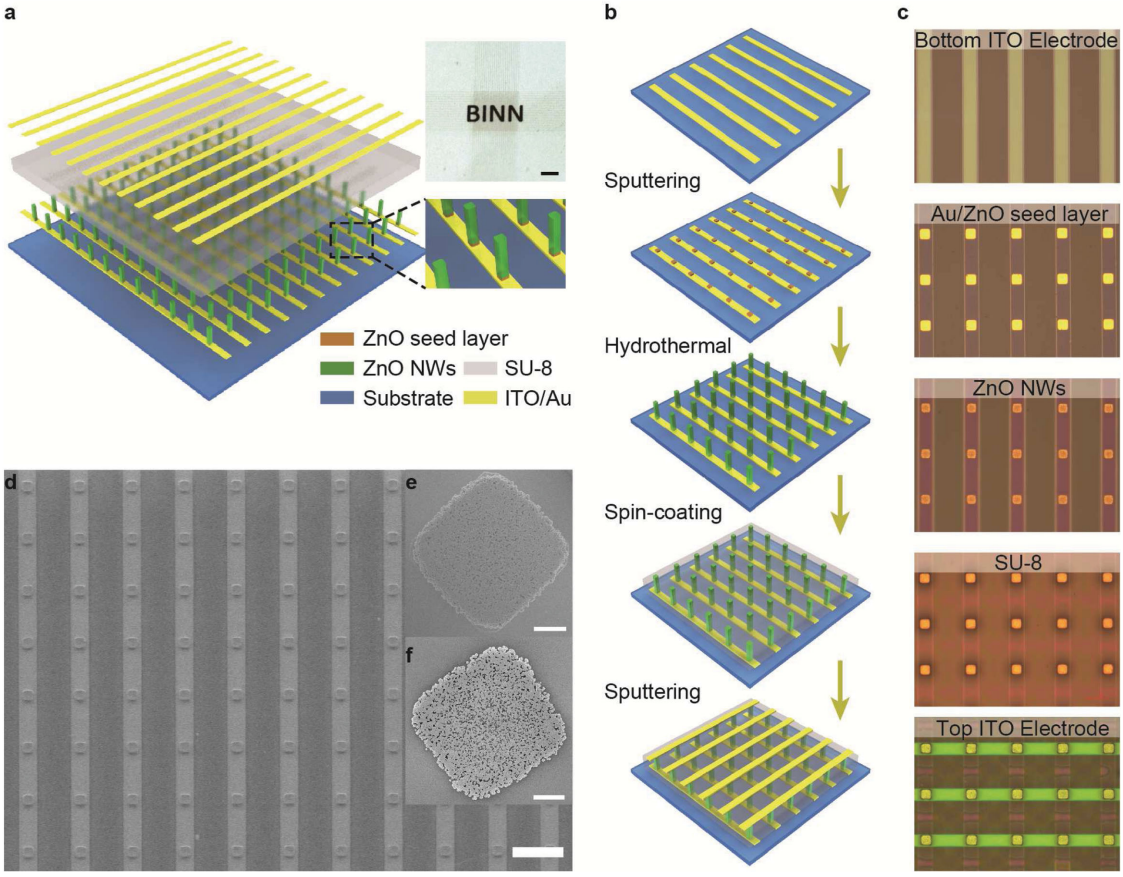

Figure 1. Structure and fabrication processes of the UV PD array. a) Schematic illustration of the structures of the ZnO NW-based UV PD array. Inset is an optical image of the as-fabricated device. The scale bar is 1 mm. b,c) Schematic illustration and the corresponding optical images of the device fabrication process. d) SEM image of the as-fabricated device before spin-coating a layer of SU-8 photoresist. The scale bar is 100 μm. ZnO NW e) before and f) after spin-coating a layer of SU-8 photoresist. The scale bar is 5 μm.

illuminations at a biased voltage of 1 V as shown in Figure 2b. A response time of 62 ms at the rising edge (Figure 2b) under 3.949 mW cm^{-2} UV illumination was derived by calculating the time interval between 10% and 90% of the steady-state values of output currents. The illumination intensity dependence of photocurrents ($I_{ph} = I_{light} - I_{dark}$) was calculated and plotted in Figure 2c. The photocurrents increased upon enhancing the illumination intensity without saturations, providing a wide dynamic detection range from 10^{-6} to 10^{-3} W cm^{-2}. The sensitivity defined as I_{ph}/I_{dark} was calculated to be 1634% under 8.36 mW cm^{-2} UV illumination. Moreover, the photoresponsivity R, which is defined as I_{ph}/P_{ill}, where I_{ph} is the photocurrent, P_{ill} is the illumination power on the PD, is also a critical parameter to evaluate the performances of the UV PD array. From Figure 2d, the photoresponsivity decreased upon increasing the illumination intensity, with the highest value of 2.64×10^4 A W^{-1} under 0.006 mW cm^{-2} UV illumination.

Sequentially characterizing the UV sensing performances of numerous pixels within the PD array was achieved by employing a multichannel testing system. The typical V–t curves of 16 pixels derived from a single-channel line scan (1×16) are presented in **Figure 3**a and Figure S3 (Supporting Information), by applying UV illumination (1.01 mW cm^{-2}) through and without a mask, respectively. The equivalent circuit of the measurements is depicted in Figure S3 (Supporting Information), indicating a serial connection among the PD, a 1 MΩ resistor, and a 3 V bias voltage applied on the top electrode, with the voltmeter measuring the voltage across the resistor. By applying UV illumination to a local region (around pixel #6 and #7) through a mask (Figure 3a), voltage responses were only observed from these two pixels as shown in Figure 3a. When UV illumination was applied to the whole device without a mask (Figure S3, Supporting Information), each pixel presented obvious voltage responses to the optical stimuli, as shown in Figure S3 (Supporting Information). In both measurements, no interference in output signals was observed from adjacent pixels, indicating the sufficient reliability and stability of the UV PD array. The statistical distribution of dark current is summarized in Figure S4 (Supporting Information) and reveals good uniformity in electrical characteristics among all pixels, with 93% of the pixels showing dark currents falling within a narrow range of 1.3 ± 0.6 μA under 1 V bias applied on the bottom voltage. Sensitive and stable UV response of the PD array enables the imaging of optical stimuli distributions by recording the electrical outputs from all pixels of the devices. As shown in Figure 3b, by increasing the UV illumination intensity, a clear "C"-shape output is derived, corresponding to the shape of the

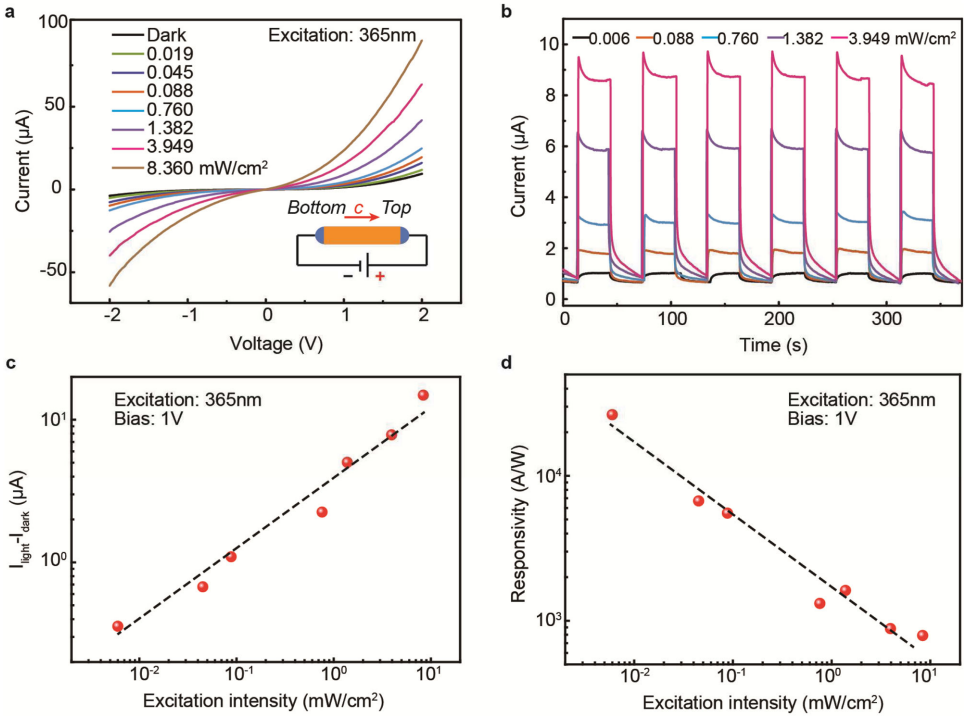

Figure 2. UV response of a single pixel without applying strains. a) *I–V* characteristics of the single pixel at dark and various 365 nm UV illumination intensities by applying a triangular wave across the device swiping from −2 to +2 V. b) Repeatable response under different UV illuminations at 1 V bias applied on the top electrode. UV illumination intensity dependences of c) photocurrent ($I_{light} - I_{dark}$) and d) photoresponsivity *R* measured at 1 V bias with top side positive.

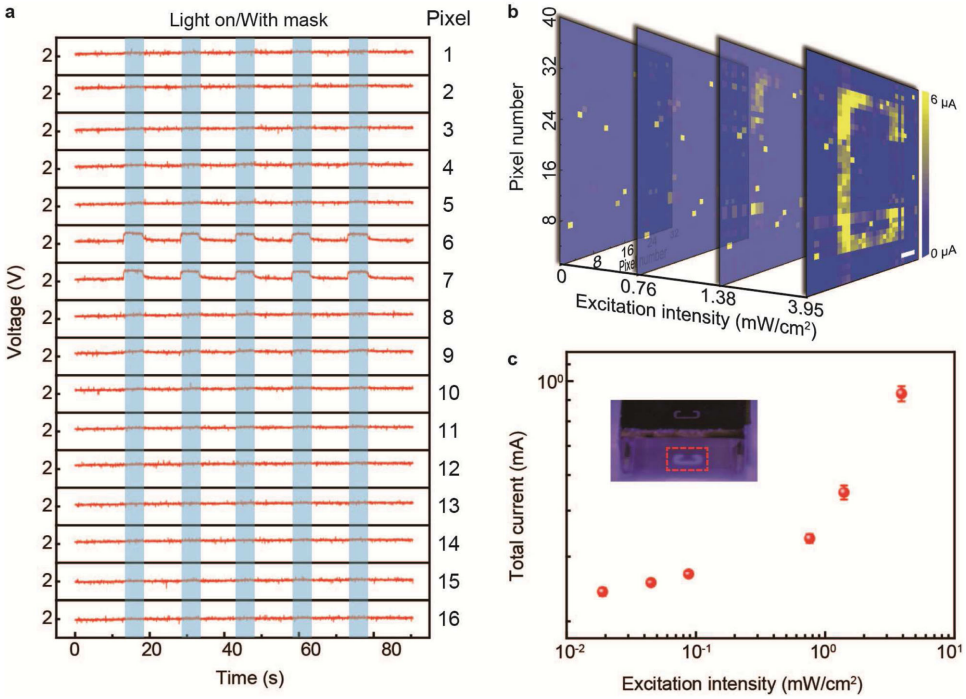

Figure 3. UV response and imaging of the illumination distributions by the PD array. a) *V–t* curves of 16 pixels derived from a single-channel line scan (1 × 16) by applying UV illuminations (1.01 mW cm^{-2}) through a mask. Pixels #6 and #7 are under UV illuminations. b) The output currents of the UV PD array to image the distribution of UV illuminations. The scale bar is 500 μm. c) Total current versus the UV illumination intensity. The inset is the optical image of the "C"-shaped UV illumination through the mask.

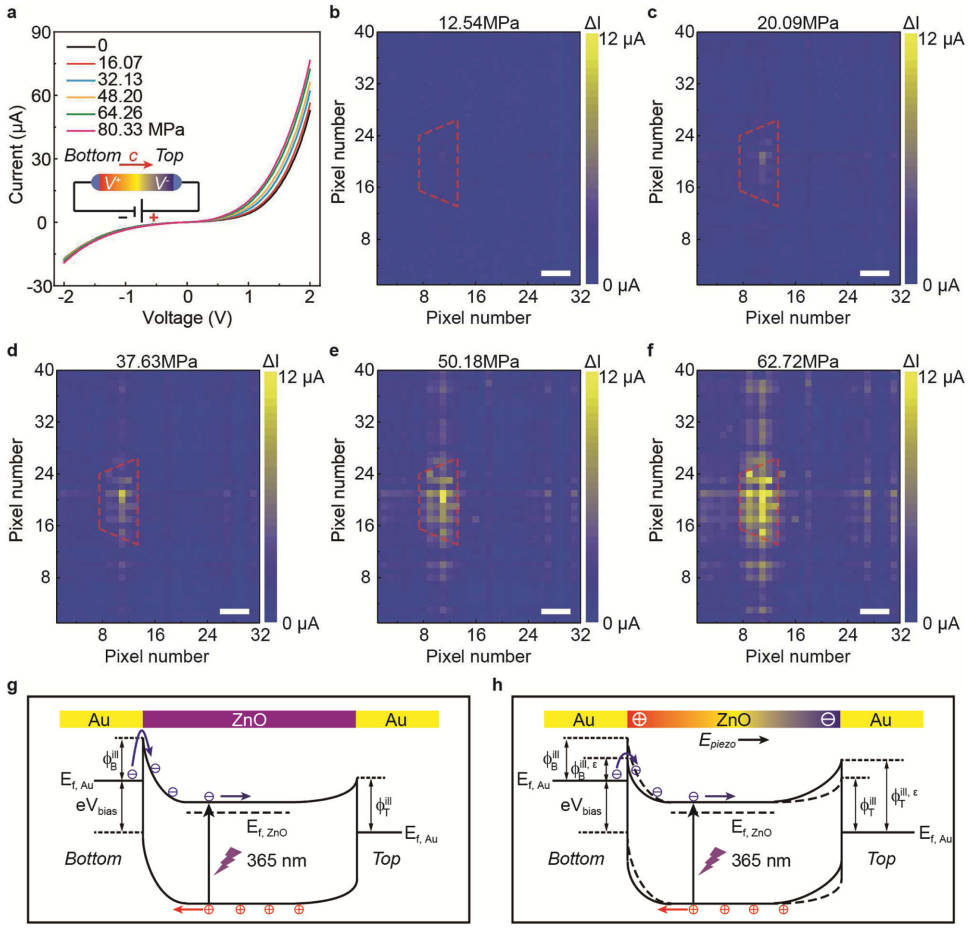

Figure 4. The piezo-phototronic effect on the UV sensing and working mechanism. a) *I–V* characteristics of a single ZnO NWs PD under various compressive strains, obtained by applying a triangular wave across the device swiping from −2 to +2 V. The current difference of the UV PD array with and without strains (I^{ε}_{light}–I^{0}_{light}) measured under b) 12.54, c) 20.09, d) 37.63, e) 50.18, and f) 62.72 MPa with the top electrodes forward biased at 1 V. The scale bar is 500 μm. Schematic energy band diagrams of Au/ZnO Schottky contact g) without and h) with compressive strains to illustrate the working mechanism of the UV PD array.

mask through which UV illuminations are applied. By subtracting the dark current as the background noise from the output currents of the UV PD array under 3.95 mW cm^{-2} illuminations, a more obvious "C"-shape output is obtained and shown in Figure S5 (Supporting Information). A new physical parameter, the total current of the UV PD array, was defined as the sum of currents from all the pixels under illuminations. The total current was calculated and summarized in Figure 3c, indicating an exponential increase with UV illumination intensities.

External strains were applied to tune/control the charge carriers' transport and thus to enhance the UV sensing performances of the PD array by introducing the piezo-phototronic effect. *I–V* characteristics of a single ZnO NWs PD without UV illuminations were investigated and summarized in **Figure 4**a, under various pressures by applying a triangular wave across the device. At +2 V, when the bottom electrode was reversely biased, the output currents increased obviously as higher pressure was applied to the device (Figure 4a); while at −2 V, when the top electrode was reversely biased, the currents remained unchanged under different straining conditions (Figure 4a). Furthermore, by applying UV illumination with a fixed intensity of 1.38 mW cm^{-2}, the current difference of the UV PD array with and without strains (I^{ε}_{light} − I^{0}_{light}) was measured under five different pressures (12.54–62.72 MPa) with the top electrodes forward biased at 1 V, as presented in Figure 4b–f, to image the strain distributions. It is obvious that better performances for imaging the strain distributions were achieved under higher pressures, indicating significant enhancements by the piezo-phototronic effect on the UV sensing of the PD array.

The working mechanism of the piezo-phototronic enhancements were carefully investigated by analyzing the energy band diagrams of Au–ZnO–Au structures, as shown in Figure 4g,h. By applying compressive strains along the *c*-axis of ZnO NWs, positive piezoelectric polarization charges were induced at the vicinity of the bottom electrodes Schottky contact to reduce the barrier height, and negative piezo-charges were presented at the top electrodes to increase the SBH, since the ZnO NWs were synthesized with *c*-axis pointing upward.[14] Considering that the electronic transport properties of metal–semiconductor–metal structures are dominated by the barrier height

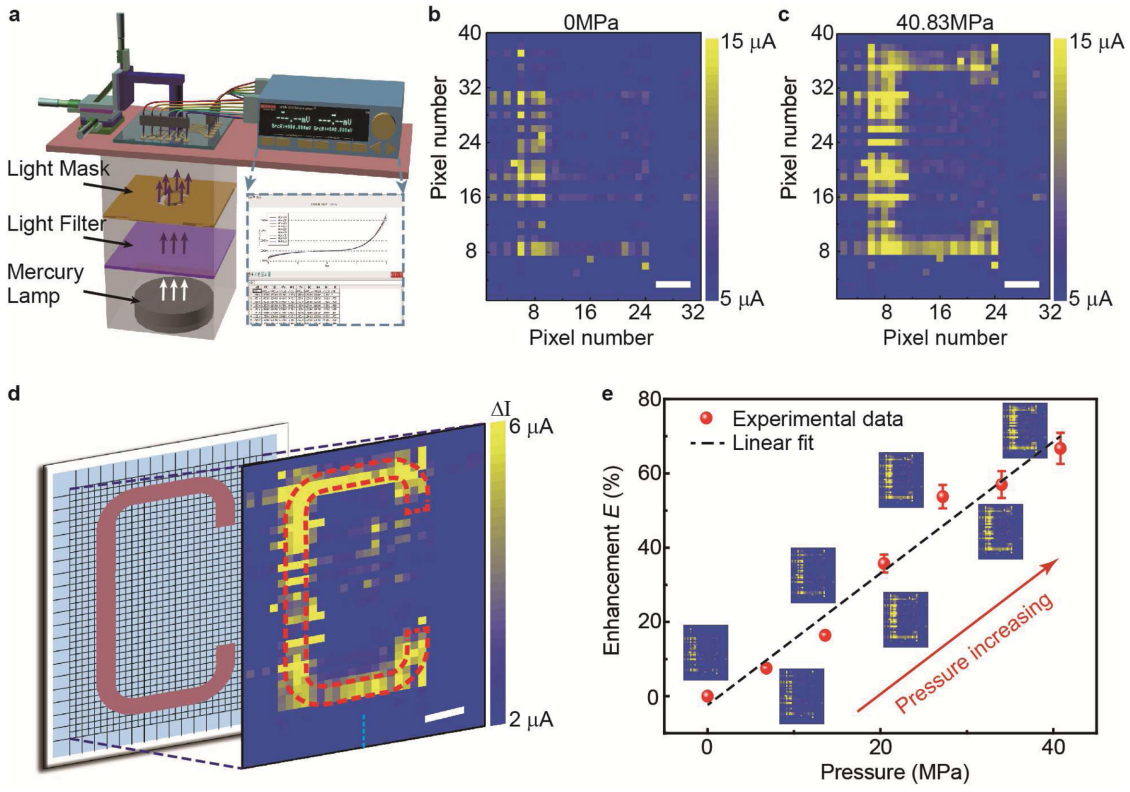

Figure 5. The enhancements on UV sensing and illumination distribution imaging by the piezo-phototronic effect. a) Experiments setup to measure the enhancements by the piezo-phototronic effect. The output currents of the UV PD array to image the distribution of UV illuminations at b) strain-free and c) 40.38 MPa pressure conditions, with illumination intensity of 1.38 mW cm^{-2} and forward biased voltage of 1 V on top electrode. d) Current difference between the data presented in (b) and (c). e) Enhancement factor E versus the applied pressures, with the corresponding output currents to image the illumination distributions at the illumination intensity of 1.38 mW cm^{-2}.

of the reversely biased Schottky contact,[15] the output currents of the UV PD array are thus controlled by the piezo-phototronic effect. With the bottom electrodes reversely biased (Figure 4g,h), the compressive strain-induced positive piezo-charges effectively reduce the SBH at local contact and enhance the carriers transport across the M–S interface. Therefore, the output currents increase with the external pressures at +2 V as shown in Figure 4a, and the UV sensing performances are significantly improved by applying more strains when the top electrode is forward biased at 1 V as shown in Figure 4b–f. On the other hand, with the top electrode reversely biased (Figure 4a at –2 V), since the corresponding SBH is already relatively high before straining, the increased barrier height by negative piezo-charges have negligible influence on the charge carriers' transport and the output currents remain unchanged with pressures at –2 V as shown in Figure 4a.

The stability and repeatability of the UV PD array operating under external pressures were investigated by repeatedly applying various strains to the device and monitoring the output currents simultaneously as shown in Figure S6 (Supporting Information). Satisfactory stability was achieved from the UV PD array, since the current of the device responded to externally applied strains sensitively and stably as increasing the pressures, and recovers to the original values as reducing the pressures back to the initial stage. The repeatability of the devices was also investigated by repeatedly applying pressures to the PD array for seven cycles, as shown in Figure S6 (Supporting Information). These results indicate that it is practical to introduce the piezo-phototronic effect to enhance the sensing performances of the UV PD array, since the devices possess stable and repeatable responses when operating under strains.

The piezo-phototronic effect enhanced UV photosensing performances of the PD array were further investigated by externally applying strains to the top surface of the device, with UV illuminations passing through the bottom glass substrate from a "C"-shape mask. **Figure 5**a schematically indicates the experiment setup; details are found in the Experimental Section. Under UV illuminations with the intensity of 1.38 mW cm^{-2}, the output currents from all the pixels of the UV PD array were measured at both strain-free and 40.83 MPa pressure and plotted in Figure 5b,c, respectively. Obviously, by introducing the piezo-phototronic effect, higher sensitivity and photoresponsivity were derived during the UV sensing as the device presenting a clearer "C"-shape output (Figure 5c). Furthermore, under 40.83 MPa pressure, the UV PD array successfully imaged the optical stimuli distributions at a relatively weak illumination intensity of 1.38 mW cm^{-2}, compared with the intensity of 3.95 mW cm^{-2} required at strain-free condition to clearly show the illumination distributions as presented in Figure 3b. By subtracting the output currents at strain-free condition (Figure 5b) from those at 40.83 MPa

pressure (Figure 5c) of the UV PD array under UV illumination of 1.38 mW cm^{-2}, a more obvious "C"-shape output was obtained, as shown in Figure 5d. The line profile of output currents were extracted from the 40 pixels in column 16 of the device (x = 16) marked in Figure 5d and plotted in Figure S7 (Supporting Information), directly indicating the amplitudes of UV sensing signals and background noise.

To better illustrate the enhancements on UV photosensing performances of the devices by the piezo-phototronic effect, an enhancement factor E was calculated and plotted in Figure 5e. The E factor is defined as $E = (\Sigma I^{\varepsilon}_{\text{light}} - \Sigma I^{0}_{\text{light}})/\Sigma I^{0}_{\text{light}}$, where $\Sigma I^{0}_{\text{light}}$ and $\Sigma I^{\varepsilon}_{\text{light}}$ represent the total currents of all the illuminated pixels at strain-free and certain straining condition, respectively. On increasing the externally applied pressures from 0 to 40.83 MPa, the E factor increases linearly from 0% to 67% under the fixed illumination intensity of 1.38 mW cm^{-2}. The corresponding output currents are presented in Figure 5e to indicate the better capability of the UV PD array to image the illumination distributions under higher pressures. The relative changes of photoresponsivity R and sensitivity S of the UV PD array under different pressures are calculated and summarized in Figure S8 (Supporting Information). Both parameters increase with the applied pressures monotonously, with the largest relative enhancements of 700% for R and 600% for S under 40.83 MPa pressure, indicating the piezo-phototronic effect enhancements on the UV sensing performances of the devices.

In conclusion, we demonstrate an UV PD array consisting of 32×40 pixels based on vertically aligned ZnO NWs. Each pixel is composed of ZnO NWs and Au nanopatterns to form a Schottky-contacted UV PD with spatial resolution of 100 μm (254 dpi), response time of 62 ms under 3.95 mW cm^{-2} UV illumination. By introducing the piezo-phototronic effect, the strain-induced piezoelectric polarization charges effectively enhance the performance of the UV PD array by 700% in photoresponsivity, 600% in sensitivity, and 280% in detection limit. The physical mechanism is carefully investigated by analyzing the energy band diagrams at the local M–S interface under mechanical deformations. This work provides a practical solution to achieving large-scale PDs with high performances by integrating NW-PDs into array configuration. The UV photodetector array may have applications in optoelectronic systems, biomedical diagnostics, adaptive optical computing, and communication.

Experimental Section

Fabrication Processes of the UV PD Array: A piece of 5 cm × 5 cm glass with 1 mm in thickness was ultrasonically cleaned by alcohol, isopropyl, and deionized water in sequence, and then dried in air for 2 h as the device substrate. First, a layer of ITO strips (150 nm in thickness, 30 μm in width, and 70 μm in spacing) was deposited as the bottom electrodes by RF magnetron sputtering (Kurt J. Lesker PVD75). Second, a layer of Au (20 nm) and a layer of ZnO (100 nm) patterns were sequentially deposited with 20 μm × 20 μm in dimension and 80 μm in spacing by RF magnetron sputtering (Kurt J. Lesker PVD75). Third, the as-deposited substrate with patterned ZnO seed layer was placed into a nutrient solution containing 20×10^{-3} M zinc nitride (Alfa Aesar) and 20×10^{-3} M hexamethylenetetramine (HMTA) (Fluka) at 90 °C for 6 h in an oven to synthesize ZnO NWs. Fourth, a layer of SU-8 photoresist was spin-coated and followed by a postbake at 135 °C for 2 h. Oxygen plasma cleaning was then applied to etch back the top part of the photoresist and expose the tips of ZnO NWs. Fifth, a layer of Au (20 nm) patterns and a layer of ITO (150 nm) strips orthogonal to the bottom electrodes were deposited as top electrodes by RF magnetron sputtering (Kurt J. Lesker PVD75). Finally, a thin layer of PVB (aladdin) was spin-coated to package the device and protect the top electrodes.

Experimental Setup and Measurements: The measurement system was customized based on a probe station (Semiprobe M-6), two piezo nanopositioning stages (Newport M-462) with a closed-loop resolution of 0.2 nm, an electronic dynamometer (ATI Nano25), and a mercury lamp (Lumen Dynamics XI120-Q) with the power of 120 W. The electrical characterization platform interfaces with the UV PD array through a customized 96-pin probe card installed on the probe station. All of the 1280 pixels were individually addressable by using the multichannel current testing system (Keithley 2612). The V–t curves from 16 pixels in a typical single-channel line scan were obtained through a multichannel voltage testing system (NI PXI-2530). A normal force/pressure was applied on the top surface of the UV PD array through a sapphire substrate controlled by the piezoelectric nanopositioning stage. The pressure was recorded by the electronic dynamometer. A 365 nm optical filter was used to obtain the parallel UV light and UV filters were applied to achieve the various illumination intensities.

Supporting Information

Supporting Information is available from the Wiley Online Library or from the author.

Acknowledgements

X.H., W.D., and R.Y. contributed equally to this work. The authors are grateful for the support received from the "thousand talents" program for the pioneer researcher and the innovation team in China, the Presidential Funding of the Chinese Academy of Sciences, and the National Natural Science Foundation of China (Nos. 51272238, 21321062, 51432005, and 61405040).

Received: May 30, 2015
Revised: August 30, 2015
Published online: October 28, 2015

[1] K. T. V. Grattan, T. Sun, *Sens. Actuators A*, **2000**, *82*, 40.
[2] a) G. Konstantatos, E. H. Sargent, *Nat. Nanotechnol.* **2010**, *5*, 391; b) G. Konstantatos, I. Howard, A. Fischer, S. Hoogland, J. Clifford, E. Klem, L. Levina, E. H. Sargent, *Nature* **2006**, *442*, 180; c) H. Kind, H. Q. Yan, B. Messer, M. Law, P. D. Yang, *Adv. Mater.* **2002**, *14*, 158; d) S. A. McDonald, G. Konstantatos, S. G. Zhang, P. W. Cyr, E. J. D. Klem, L. Levina, E. H. Sargent, *Nat. Mater.* **2005**, *4*, 138; e) J. Qi, X. Zhou, D. Yang, W. Qiao, D. Ma, Z. Y. Wang, *Adv. Funct. Mater.* **2014**, *24*, 7605.
[3] a) Q. Yang, X. Guo, W. H. Wang, Y. Zhang, S. Xu, D. H. Lien, Z. L. Wang, *ACS Nano* **2010**, *4*, 6285; b) S. Liu, J. F. Ye, Y. Cao, Q. Shen, Z. F. Liu, L. M. Qi, X. F. Guo, *Small* **2009**, *5*, 2371.
[4] a) X. Q. Liu, L. Jiang, X. M. Zou, X. H. Xiao, S. S. Guo, C. Z. Jiang, X. Liu, Z. Y. Fan, W. D. Hu, X. S. Chen, W. Lu, W. P. Hu, L. Liao, *Adv. Mater.* **2014**, *26*, 2919; b) M. Engel, M. Steiner, P. Avouris, *Nano Lett.* **2014**, *14*, 6414.
[5] a) X. Liu, L. Gu, Q. Zhang, J. Wu, Y. Long, Z. Fan, *Nat. Commun.* **2014**, *5*, 4007; b) J. Zhou, Y. Gu, Y. Hu, W. Mai, P. H. Yeh, G. Bao, A. K. Sood, D. L. Polla, Z. L. Wang, *Appl. Phys. Lett.* **2009**, *94*, 191103; c) Y. Jin, J. Wang, B. Sun, J. C. Blakesley, N. C. Greenham, *Nano Lett.* **2008**, *8*, 1649.

[6] a) C. Soci, A. Zhang, B. Xiang, S. A. Dayeh, D. P. R. Aplin, J. Park, X. Y. Bao, Y. H. Lo, D. Wang, *Nano Lett.* **2007**, *7*, 1003; b) E. Monroy, F. Omnes, F. Calle, *Semicond. Sci. Technol.* **2003**, *18*, R33.

[7] a) W. Kim, K. S. Chu, *Phys. Status Solidi A* **2009**, *206*, 179; b) M. W. Chen, C. Y. Chen, D. H. Lien, Y. Ding, J. H. He, *Opt. Express* **2010**, *18*, 14836; c) Z. N. Wang, R. M. Yu, C. F. Pan, Y. Liu, Y. Ding, Z. L. Wang, *Adv. Mater.* **2015**, *27*, 1553.

[8] a) Z. L. Wang, R. S. Yang, J. Zhou, Y. Qin, C. Xu, Y. F. Hu, S. Xu, *Mater. Sci. Eng. R,* **2010**, *70*, 320; b) M. Eichenfield, J. Chan, R. M. Camacho, K. J. Vahala, O. Painter, *Nature* **2009**, *462*, 78.

[9] Z. L. Wang, *Adv. Mater.* **2012**, *24*, 4632.

[10] a) L. Dong, S. M. Niu, C. F. Pan, R. M. Yu, Y. Zhang, Z. L. Wang, *Adv. Mater.* **2012**, *24*, 5470; b) C. F. Pan, S. M. Niu, Y. Ding, L. Dong, R. M. Yu, Y. Liu, G. Zhu, Z. L. Wang, *Nano Lett.* **2012**, *12*, 3302; c) X. D. Wang, H. L. Zhang, R. M. Yu, L. Dong, D. F. Peng, A. H. Zhang, Y. Zhang, H. Liu, C. F. Pan, Z. L. Wang, *Adv. Mater.* **2015**, *27*, 2324.

[11] a) F. Zhang, S. M. Niu, W. X. Guo, G. Zhu, Y. Liu, X. L. Zhang, Z. L. Wang, *ACS Nano* **2013**, *7*, 4537; b) Z. Zhang, Q. L. Liao, Y. H. Yu, X. D. Wang, Y. Zhang, *Nano Energy* **2014**, *9*, 237; c) R. M. Yu, W. Z. Wu, C. F. Pan, Z. N. Wang, Y. Ding, Z. L. Wang, *Adv. Mater.* **2015**, *27*, 940; d) R. Bao, C. Wang, L. Dong, R. Yu, K. Zhao, Z. L. Wang, C. Pan, *Adv. Funct. Mater.* **2015**, *25*, 2884; e) X. N. Wen, W. Z. Wu, Z. L. Wang, *Nano Energy* **2013**, *2*, 1093.

[12] Y. Liu, Q. Yang, Y. Zhang, Z. Y. Yang, Z. L. Wang, *Adv. Mater.* **2012**, *24*, 1410.

[13] Z. M. Liao, K. J. Liu, J. M. Zhang, J. Xu, D. P. Yu, *Phys. Lett. A* **2007**, *367*, 207.

[14] a) J. Jasinski, D. Zhang, J. Parra, V. Katkanant, V. Leppert, *Appl. Phys. Lett.* **2008**, *92*, 093104; b) S. Xu, C. Xu, Y. Liu, Y. F. Hu, R. S. Yang, Q. Yang, J. H. Ryou, H. J. Kim, Z. Lochner, S. Choi, R. Dupuis, Z. L. Wang, *Adv. Mater.* **2010**, *22*, 4749; c) C. F. Pan, L. Dong, G. Zhu, S. M. Niu, R. M. Yu, Q. Yang, Y. Liu, Z. L. Wang, *Nat. Photonics* **2013**, *7*, 752; d) W. Z. Wu, X. N. Wen, Z. L. Wang, *Science* **2013**, *340*, 952.

[15] a) Z. Fan, J. G. Lu, *Appl. Phys. Lett.* **2005**, *86*, 123510; b) R. M. Yu, L. Dong, C. F. Pan, S. M. Niu, H. F. Liu, W. Liu, S. Chua, D. Z. Chi, Z. L. Wang, *Adv. Mater.* **2012**, *24*, 3532.